IJPSR (2019), Volume 10, Issue 6 **(Research Article)**

INTERNATIONAL JOURNAL OF PHARMACEUTICAL SCIENCES AND RESEARCH

Received on 15 September 2018; received in revised form, 04 December 2018; accepted, 06 December 2018; published 01 June 2019

A FACILE NOVEL SYNTHESIS OF ThO_2/Fe_3O_4 NANOCOMPOSITE WITH ENHANCED PHOTOCATALYTIC ACTIVITY FOR THE DEGRADATION OF MALACHITE GREEN UNDER VISIBLE LIGHT IRRADIATION

Ramya Arumugam [1], Prakash Periakaruppan [*1] and Rayappan Selvanathan [2]

Department of Chemistry [1], Thiagarajar College, Madurai - 625009, Tamil Nadu, India.
Department of Chemistry [2], Arul Anandar College, Karumathur - 625514, Tamil Nadu, India.

Keywords:

ThO_2/Fe_3O_4 nanocomposite, Malachite green, Photocatalysis, Catalyst, the Degradation mechanism

Correspondence to Author:
Prakash Periakaruppan

Department of Chemistry, Thiagarajar College, Madurai - 625009, Tamil Nadu, India.

E-mail: kmpprakash@gmail.com

ABSTRACT: An innovative magnetically separable ThO_2/Fe_3O_4 nanocomposite was successfully synthesized by hydrothermal method. The synthesized ThO_2/Fe_3O_4 nanocomposite was characterized by UV-DRS, FT-IR, XRD, HR-TEM, BET, and TGA techniques. XRD and HR-TEM images displayed the overall spherical shape and confirmed the formation of well crystalline ThO_2/Fe_3O_4 nanocomposite. The catalytic efficiency of ThO_2/Fe_3O_4 was explored for the removal of malachite green dye (MG) from the aqueous phase. The degradation efficiency of about 99.53% was obtained, and the degradation reaction was maximal at pH 5. The results revealed that the synthesized ThO_2/Fe_3O_4 nanocomposite showed enhanced photocatalytic activity compared to the ThO_2 and Fe_3O_4 samples. Based on obtained results, the most plausible mechanism for removal MG has been proposed. The ThO_2/Fe_3O_4 photocatalyst remained a robust performer even after five cycles. This nanocomposite is an effective visible light responsive material which can be used for the removal of various organic pollutants from the environment.

INTRODUCTION: Contamination by organic pollutants has become a major environmental concern with industrial development and increases in the human population [1, 2]. In recent years, dyes are also an important class of pollutants that can be toxic and even carcinogenic to human beings [3]. Among other pollutants, malachite green (MG) is a kind of triphenylmethane dye which has been widely used in the production of ceramics, leather, textile industry, food coloring, cell coloring, wool, jute, paper, acrylic industry, parasiticide, fungicide and bactericide in aquaculture industries globally [4]. However, malachite green has an adverse effect on the reproductive and immune system, and it shows potential genotoxic, carcinogenic effects, damaging effects on gill, intestine, kidney, liver, and it causes anemia, thyroid abnormalities [5]. Therefore, it is necessary to find an effective method to remove MG from wastewater in an efficient and cost-effective way before its release into the environment [6].

In recent years, it has been proven that the photocatalytic degradation technology is an effective method for environmental remediation and efficient way for the removal of organic waste material from water system [7]. For photocatalytic system, the nanosized metal oxides and their composites are developed because they possess high surface area and exhibit excellent physical and chemical properties due to its promising application in the energy production and environment-friendly

QUICK RESPONSE CODE

DOI: 10.13040/IJPSR.0975-8232.10(6).2902-10

The article can be accessed online on www.ijpsr.com

DOI link: http://dx.doi.org/10.13040/IJPSR.0975-8232.10(6).2902-10

and economical approach for the degradation of organic pollutants persisting in our environment [8]. Recently, actinide - based nanomaterials have attracted more attention as they are considered very promising for the preparation of innovative nuclear fuels and highly efficient photocatalysts [9, 10, 11]. Therefore, the target synthesis of actinide oxide nanoparticles with specific sizes and shapes is of great importance for both applied and fundamental research. Among actinide oxides, ThO_2 has attracted increasing attention in recent years due to its usage as ceramics, sensors, solid electrolytes, optical materials, traditional nuclear industry, and catalysts [12]. However, a single photocatalyst always suffers from the drawback of deficient separation and transfer of charge carriers, which counteracts the high-activity performance of photocatalysts [13].

Among various photocatalysts, an iron oxide containing transition metal oxides are efficient in photocatalysis. Electron transport at the interface between two semiconductors is one of the important aspects for the design of this novel material. Thus, the photogenerated charge carriers, electrons, and holes are easily separated and are utilized for redox reaction [14, 15]. Recently, ThO_2 particles were doped with iron oxides particles because of their non-toxicity, low cost, compatible magnetic and electrochemical properties, which low cost, physical and chemical stability, high catalytic activity, environmental friendliness and ease of availability [16, 17].

Herein, we have designed and developed a nano-structured ThO_2/Fe_3O_4 nanocomposite for the photocatalytic degradation of MG dye. The effects of the concentration of malachite green, pH value, and the concentration of photocatalyst on the degradation efficiency have been investigated. The fabricated ThO_2/Fe_3O_4 nanoparticles showed excellent photocatalytic activity for the degradation of MG dye under visible light irradiation.

EXPERIMENTAL:

Materials and Methods: All chemicals were analytical grade and used as purchased without further purification. $Th(NO_3)_4.5H_2O$ and $FeCl_3.6H_2O$, ethylene glycol, sodium acetate, trisodium citrate, toluene, and ethanol were purchased from Sigma Aldrich. Deionized (DI) water was used throughout the synthesis process.

Synthesis of ThO_2 Nanoparticles: In the hydro-thermal preparation, 1.5 g of $Th(NO_3)_4.5H_2O$ powder was weighed into a 50 ml Teflon lined stainless steel autoclave, and subsequently 40 ml of toluene was added. The autoclave was sealed and maintained at 180 °C for 24 h in an electric oven, then cooled to room temperature naturally. The resulting precipitate was filtered, washed with ethanol and DI water for several times, and dried at 80 °C.

Synthesis of Fe_3O_4 Nanoparticles: The Fe_3O_4 magnetic nanoparticles were synthesized *via* a hydrothermal method according to previous report [18]. Briefly, $FeCl_3.6H_2O$ (3.3 g) and trisodium citrate (0.6 g) were dissolved in ethylene glycol (60 ml) to form a clear solution, followed by the addition of sodium acetate (6.0 g). The mixed solution was stirred vigorously for 30 min and then sealed in a Teflon lined stainless steel autoclave (100 ml capacity). The autoclave was heated and maintained at 200 °C for 10 h, and then allowed to cool to room temperature. The products were collected and washed several times with ethanol, DI water, and vacuum dried at 60 °C overnight.

Synthesis of ThO_2/Fe_3O_4 Nanocomposite: ThO_2 nanoparticles and Fe_3O_4 nanoparticles were added into absolute ethanol and ultrasonically dispersed for 10 min. After being stirred for 1 h at 75 ºC, the precipitate was separated, washed and dried at 80 ºC for 6 h. The obtained ThO_2/Fe_3O_4 product was calcined at 500 ºC for 2 h.

Characterization:

Material Characterization: The UV-Vis diffuse reflectance spectroscopy (UV-DRS) was recorded on a UV- 2400 spectrophotometer (Shimadzu Corporation, Japan) using $BaSO_4$ as the reference. Fourier transform infrared spectra (FT-IR) were recorded with a JASCO FT-IR 460 plus spectrometer. XRD analysis was carried out using Cu Ka radiation (k = 1.5418 Å) on a JEOL JDX 8030 X-ray diffractometer. The morphology of the material was ascertained High-resolution transmission electron microscopy and the corresponding selected- area electron diffraction (HR-TEM/ SAED) was carried out on a JEOL JEM 2100 analytical scanning transmission electron microscope. The samples for TEM were prepared by placing a drop of the prepared solution on

carbon-coated copper grids, followed by drying. Photodegradation experiments were performed in a HEBER immersion type photoreactor (HIPR-MP125). TGA of samples was carried out with a TGA-50, SHIMADZU thermogravimetric analyzer at a heating rate of 10 ºC min^{-1} up to 800 ºC under nitrogen gas.

Photodegradation Experiments: In the evaluation of photodegradation reaction, the experiment was conducted in a cylindrical immersion type photoreactor. The initial concentration of MG dye was taken 2×10^{-5} M, and the 25 mg of the ThO_2/ Fe_3O_4 nanocomposite was added in the dye solutions to form a slurry. The reaction mixture was stirred in the dark for a certain time to establish the adsorption-desorption equilibrium of the dye molecules and dissolved water with the catalyst surface. Photolysis experiment of MG dye in the absence of photocatalyst under visible light was carried out by the aforementioned procedure. Further, the photocatalytic experiment was initiated by illuminating the system with visible light and after specific time intervals; certain aliquots of solution were withdrawn out with syringe at pre-determined time intervals, the dispersion was drawn and separated immediately by the adscititious magnet and collected. The residual amount of MG dye in the solution was analyzed using a UV-Vis spectrophotometer (JASCO V-530) based on its characteristic optical absorption at 619 nm. The decolorization efficiency (%) is calculated as:

$$\text{Photodegradation (\%)} = C_0 - C / C_0 \quad \text{.....1}$$

Here, C is the absorption of MG solution at irradiation time of 't' min and C0 is the initial absorption at t = 0 min.

RESULTS AND DISCUSSION:

UV-DRS: To understand the band structures of these materials, optical absorption study has been carried out in the wavelength (λ) range 200-900 nm, as shown in **Fig. 1**. The results reveal that the absorption edge shifted to longer wavelengths as the ThO_2 was doped into the surface of Fe_3O_4. The direct band gap was calculated from the UV-DRS spectra. We used the following formula for calculating band gaps from obtained diffuse reflectance spectra:

$$E = h*C / \lambda \quad \text{.....2}$$

Where, h is Planck's constant, C is the speed of light, and λ is cut off wavelength of recorded spectral data.

Fig. 1a-c shows the UV-DRS spectra of the ThO_2, Fe_3O_4 and ThO_2/Fe_3O_4 nanocomposite. The ThO_2, Fe_3O_4 nanoparticles and ThO_2/Fe_3O_4 nano-composite show the adsorption edge of 300, 450 and 475 nm, corresponding to a band gap of 1.8 eV, 2.2 eV, and 2.7 eV respectively, which signifies its photocatalytic activity under visible-light irradiation. The absorption of the ThO_2/Fe_3O_4 nanocomposites within the visible-light range significantly increased, and a red shift in comparison with the pure Fe_3O_4. These results are attributed to the interaction between the ThO_2 and Fe_3O_4 nanoparticles in the composite system. The enhanced light absorption of the ThO_2/Fe_3O_4 nanocomposite leads to the generation of more photoinduced electron-hole pairs under visible-light irradiation, which subsequently results in enhanced photocatalytic activity.

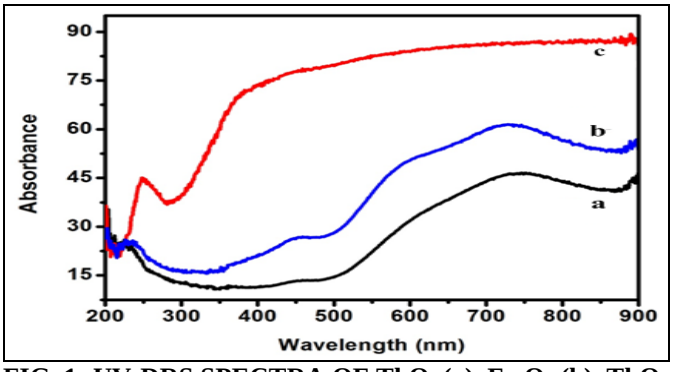

FIG. 1: UV-DRS SPECTRA OF ThO_2 (a), Fe_3O_4 (b), ThO_2 / Fe_3O_4 (c) NANOCOMPOSITE

FT - IR Spectroscopy: FT - IR measurements provided further evidence for the formation of ThO_2/Fe_3O_4 nanocomposite. **Fig. 2** illustrates the FT-IR spectra of ThO_2 (a), Fe_3O_4 (b) and ThO_2/ Fe_3O_4 (c) nanocomposite. For all the samples, most typical band at 3420 cm^{-1} was assigned to the stretching vibration of OH group and appearance of bands around 2927 cm^{-1} and 2332 cm^{-1} was attributed to stretching in C-H group respectively. The magnetite NPs can be seen by wide strong absorption band between 580 and 630 cm^{-1}, especially for Fe-O bond of bulk magnetite at 576 cm^{-1} [19] as well as those at 1620 cm^{-1} can be ascribed to carboxylate groups [20]. This indicates that magnetic Fe_3O_4 nanoparticles are capped with citrate groups that derived from the introduction of

trisodium citrate during the solvothermal synthesis. These FT-IR spectra provided useful information that the Fe_3O_4 were successfully bound to the ThO_2.

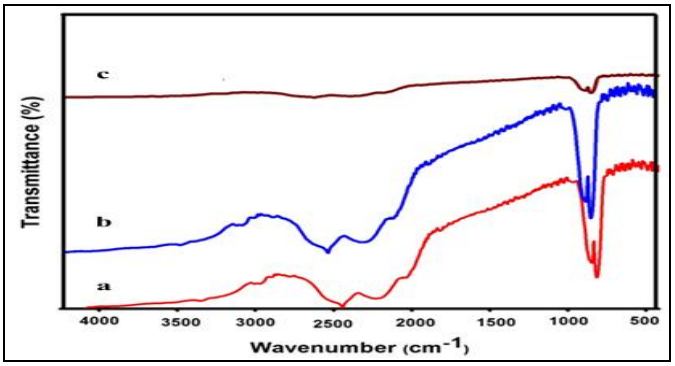

FIG. 2: FT-IR SPECTRA OF ThO_2 (a), Fe_3O_4 (b), Fe_3O_4/ ThO_2 (c) NANOCOMPOSITE

XRD: The phase and crystalline composition of the as-prepared Fe_3O_4 and ThO_2 nanocomposite are examined by XRD measurements. The powder XRD pattern of the precursor is shown in **Fig. 3** Fe_3O_4 (a), ThO_2 (b) and ThO_2/Fe_3O_4 (c). All the diffraction patterns obtained were indexed to the characteristic peaks of ThO_2 (JCPDS card no. 65-7222). Also a typical XRD pattern of the Fe3O4showed diffraction peaks at 2θ = 27.56°, 30.07°, 35.42°, 37.05°, 43.05°, 56.9°, 62.52°, 73.96° respectively corresponding to the (111), (220), (311), (222), (400), (333), (440) and (533) reflection face-centered cubic lattice of Fe_3O_4, which match well with the data from the JCPDS file (Card no. 82-1533) for Fe_3O_4. It was observed that Fe_3O_4/ ThO_2 shows the diffraction peaks at 2θ = 0.19 and 0.14° respectively.

The average crystalline structure was calculated from the most intense peak of 220 and it was found to be 8nm respectively. The XRD patterns that can be seen there are no additional peaks, implying the absence of impurity phases in the sample. This confirms the mesoporous and crystalline nature of the material. The average crystallite size of the synthesized ThO_2/Fe_3O_4 nanocomposites calculated by the XRD data according to Scherrer's equation.

$$D = k \lambda / \beta \cos \theta \quad \text{.....3}$$

Where, d is the thickness of crystallite (nm), k is a constant dependent on the crystallite shape, λ is the X-ray wavelength (nm), B is the full width at half max in radians, and θ is the Bragg angle of the 2θ peak.

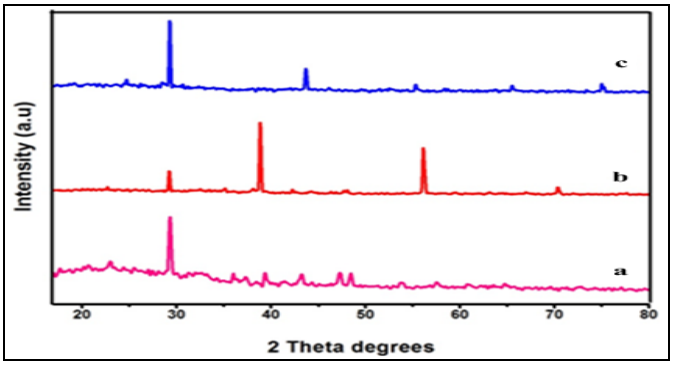

FIG. 3: (a-c) XRD PATTERN OF Fe_3O_4, ThO_2, AND ThO_2/Fe_3O_4 NANOCOMPOSITE

TEM: The morphology, particle size, and structure of the products were characterized by TEM. The TEM images of different magnifications of ThO_2/ Fe_3O_4 nanocomposite are shown in **Fig. 4a-d**. To investigate the stability of Fe_3O_4 attached on the ThO_2 nanoparticles, a leaching test was conducted through treating the as-synthesized ThO_2/Fe_3O_4 sample fully dispersed with ethanol under sonication. Even after sonication for 30 min, the Fe_3O_4 nanoparticles are still firmly anchored on the ThO_2, suggesting the strong interaction between ThO_2 and Fe_3O_4. The morphology of pure ThO_2/ Fe_3O_4 nanocomposite shows spherical shape with uniform sizes and face-centered cubic structure. The average crystallite size of ThO_2/Fe_3O_4 nanocomposite is 8 nm, respectively. **Fig. 4d** illustrates Fe_3O_4 nanoparticles appearing black and the ThO_2 nanoparticles with a lighter color as observed for ThO_2/Fe_3O_4 nanocomposite. It is noticeable that ThO_2 nanoparticles are uniformly coated on the surface of the Fe_3O_4 nanoparticles.

The TEM images for the crystalline nature of ThO_2/Fe_3O_4 nanocomposite is displayed in **Fig. 5a-b**. The selected area electron diffraction (SAED) pattern of ThO_2/Fe_3O_4 nanocomposite is presented in **Fig. 5c**. The SAED pattern revealed several bright continuous concentric rings attributed to the diffraction from the (111), (220), (222), (400), (333) and (533) planes of ThO_2/Fe_3O_4, consistent well with the XRD data. The SAED pattern indicates the well crystalline nature of the prepared photocatalysts. EDX spectroscopy was employed to investigate the chemical composition and purity of the ThO_2/Fe_3O_4 nanocomposite. **Fig. 5d** shows that the corresponding results of the EDX pattern of the ThO_2/Fe_3O_4 nanoparticles contain four elements of Fe, Th, Cu, and O.

The energy-dispersive X-ray spectroscopy (EDS) demonstrates the coexistence of Fe, Th, O elements, which indicate the formation of ThO_2 and Fe_3O_4 nanocomposite.

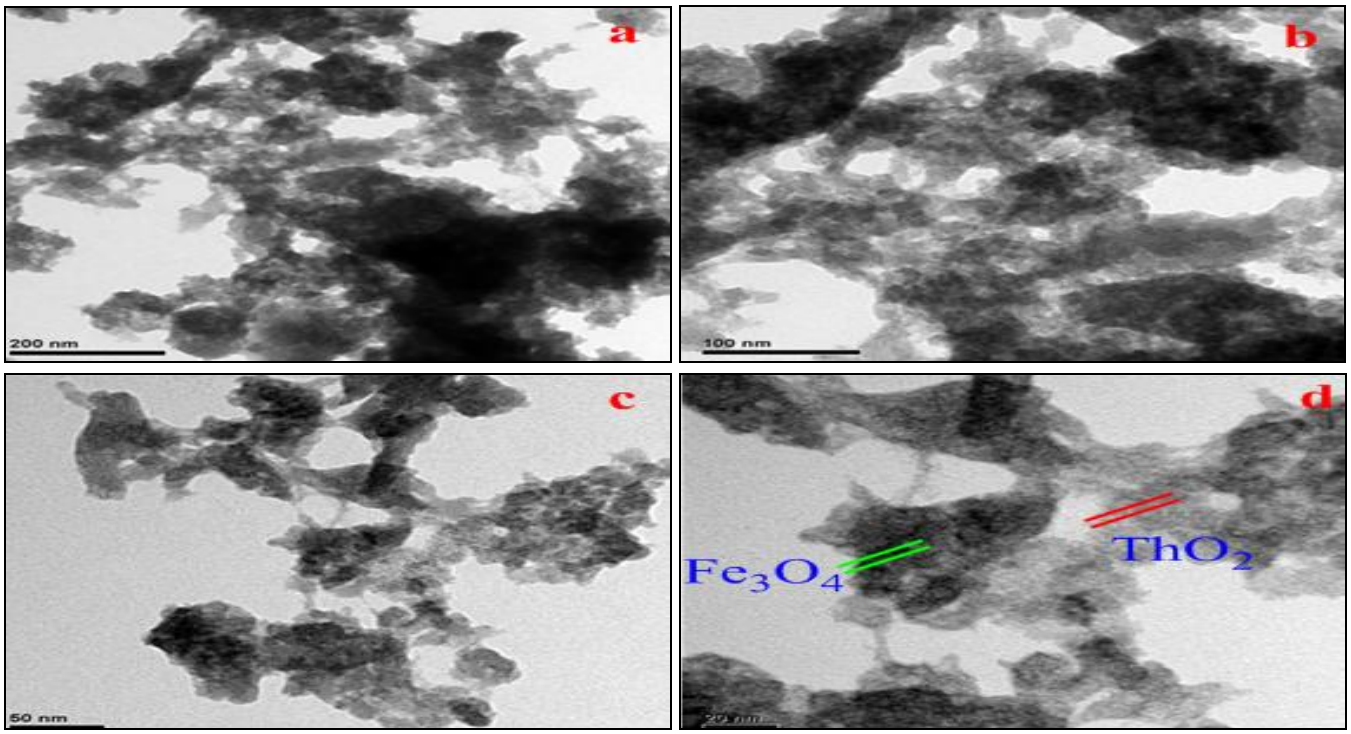

FIG. 4: (a-d) HR-TEM IMAGES OF DIFFERENT MAGNIFICATIONS OF ThO_2/Fe_3O_4 NANOCOMPOSITE

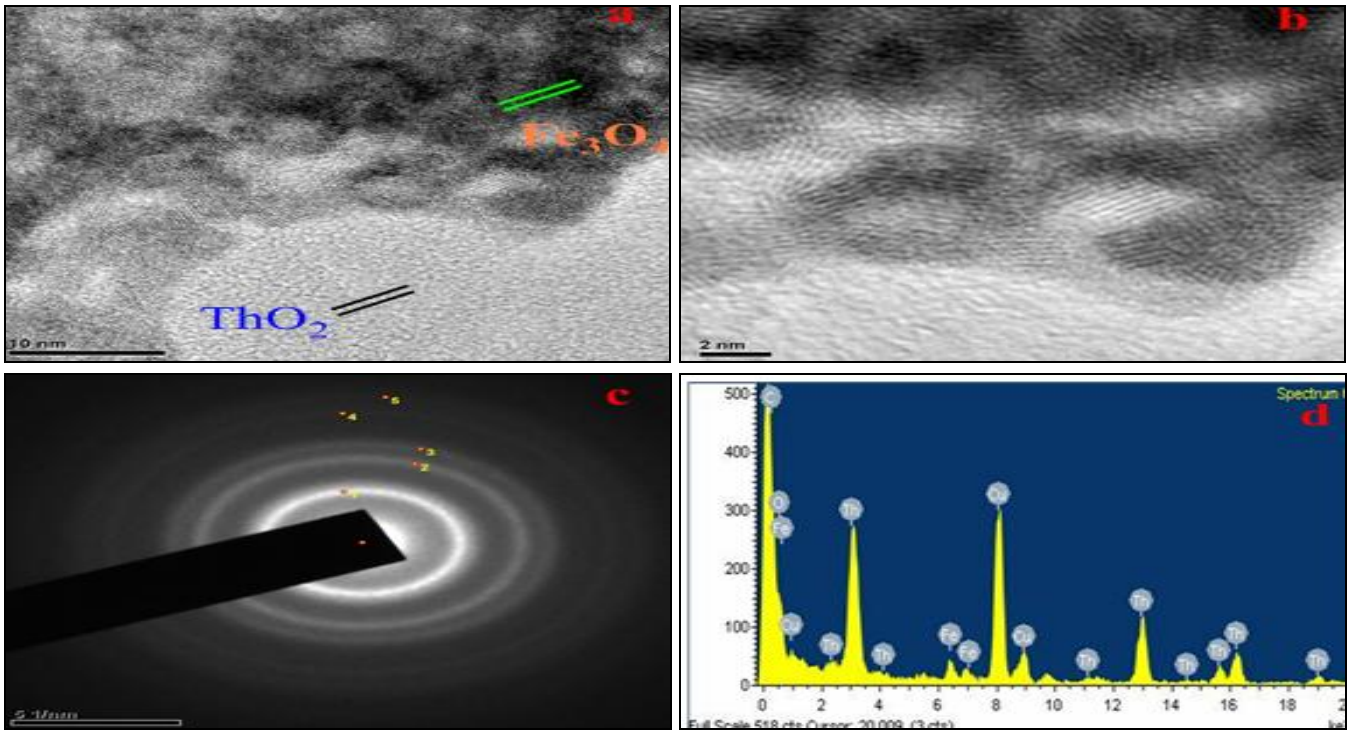

FIG. 5: (a, b) HR-TEM IMAGES OF CRYSTALLINE NATURE OF ThO_2/Fe_3O_4 NANOCOMPOSITE, (c) SAED PATTERN OF ThO_2/Fe_3O_4 NANOCOMPOSITE, (d) EDX SPECTRUM OF ThO_2/Fe_3O_4 NANOCOMPOSITE

BET: The specific surface area, pore volume, and size analysis were calculated using the Brunauer-Emmet-Teller (BET) method. A typical nitrogen adsorption-desorption isotherm of all the photocatalysts are shown in **Fig. 6**. All the samples exhibit type IV nitrogen sorption isotherm with a capillary condensation step in the relative pressure (P/P_0) range 0-1.0, indicating a well-developed mesoporosity [21]. The BET surface area of the nanocomposite was found to be 165.66 m^2/g,

calculated by the linear part of the BET plot. **Fig. 6a** (insert) shows that the total pore volume was observed by 0.55794 cm^3g. The surface area, pore size, and pore volume of all the photocatalysts are presented in **Table 1**. Mesoporous structure and relatively high surface area could be responsible for its high photocatalytic activity.

TGA: The TGA plot in **Fig. 7** shows the ThO_2/ Fe_3O_4 nanocomposite, which shows a steady weight loss in the temperature range of 25-700 ºC. The first weight loss (40.84%) was observed between 36-200 ºC, which can be attributed to the removal of physisorbed water molecules.

The second weight loss (8.77%) was occurring in the range of 270 to 400 ºC due to the decomposition of bioorganic compounds in ThO_2/ Fe_3O_4 nanocomposite.

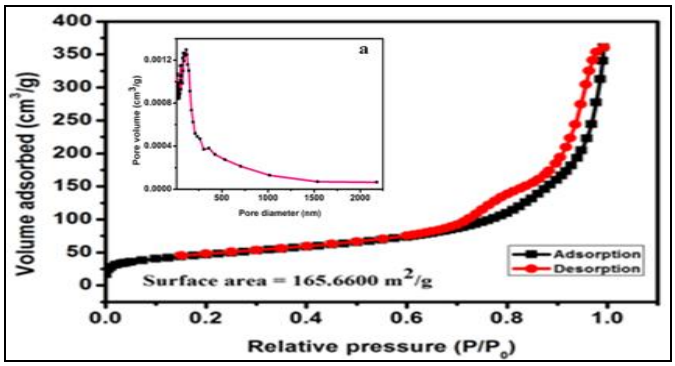

FIG. 6: N_2 ADSORPTION-DESORPTION ISOTHERM AND INSERT (FIG. a) PORE-SIZE DISTRIBUTIONCURVE OF THE ThO_2/Fe_3O_4 NANOCOMPOSITE

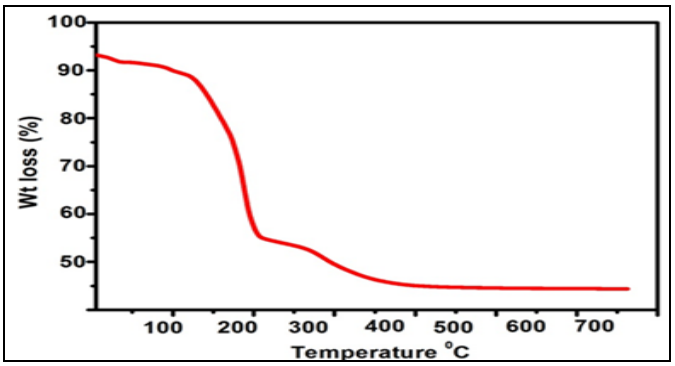

FIG. 7: TGA ANALYSIS OF ThO_2/Fe_3O_4 NANOCOMPOSITE

TABLE 1: SURFACE AREA, PORE VOLUME, PORE SIZE OF SYNTHESIZED THO_2/FE_3O_4 NANOCOMPOSITE

Sample name	Surface area (m^2/g) BET result	Pore volume (cm^3/g) BET result	Pore size (nm) BET result	Crystalline size (nm) XRD result
ThO_2/Fe_3O_4 nanocomposite	165.66	0.55794	1.347	8

Above the temperature of 400 ºC, the pure ThO_2 / Fe_3O_4 only exists, which is stable up to 600 ºC.

Photocatalytic Activity:

Effect of Time: Fig. 8 shows the changes in the MG absorption spectra during photocatalytic degradation with ThO_2/Fe_3O_4 at different irradiation times varying from 0 to 40 min. More than 75% of the MG is degraded within 40 min.

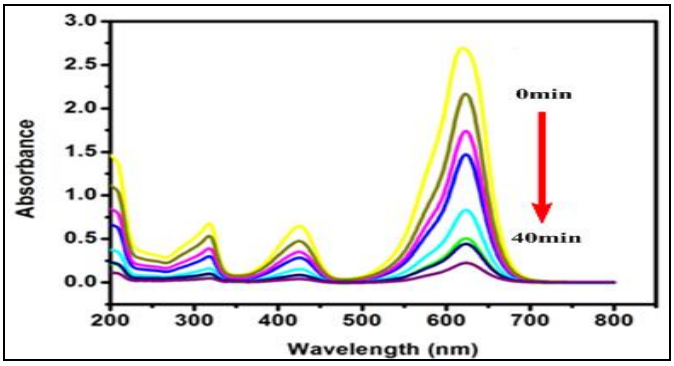

FIG. 8: PHOTOCATALYTIC DEGRADATION OF MG AT DIFFERENT TIME INTERVALS (0-40 min) USING ThO_2/Fe_3O_4 NANOCOMPOSITE

The results show that the absorption of the visible band at 618 nm decreased and a hypsochromic shift occurred simultaneously with increasing illumination time. The hypsochromic shift may be caused by an N-demethylation process. The absorbance peaks at 425 and 315 nm have declined, which indicates that the entire conjugated chromophore structure of MG has been destroyed [22].

Effect of pH on the Photodegradation of MG: The influence of different pH (3, 5, 7, and 9) value on the degradation efficiency of MG was investigated, which is shown in **Fig. 9**. The natural pH value of MG solution was found to be 5.2. The pH value was adjusted using dilute HCl or dilute NaOH solution for the experiment. The effect of pH on the degradation of MG was examined by changing the pH from 3, 5, 7 and 9 at a fixed amount of catalyst (0.25 g/L) and constant MG concentration (10 mg/L). **Fig. 9a** shows the effect of pH on the photodegradation of MG solution. At pH 5, it is observed that the absorption band of the MG is 619 nm. Since, the color from deep green changes to colorless, there is a rapid decrease with a slight hypochromic shift which is found at 619

nm, and there is no new absorption band in the UV range. It indicates that there would be a cleavage of the conjugated chromophore structure of the MG which would have occurred because of the formation of N-de-methylated intermediates. In the acidic pH 5, the absorption peak at 619 nm confirmed that there is adsorption of MG on ThO_2/Fe_3O_4 catalyst surface. It is found that degradation occurs (99.53%) within 40 min at pH 5. The electrons in the conduction band can be captured by the soluble O_2, and the holes can be trapped by the surface hydroxyl, these process resulting in the formation of hydroxyl radical species ($^{\bullet}OH$), which are easily generated by oxidizing more hydroxide ions in acidic solution. Thus, the efficiency of the degradation process is enhanced in the acidic medium, especially at pH 5. Thus, the acidic medium favors the complete degradation of MG on the surface of the catalyst.

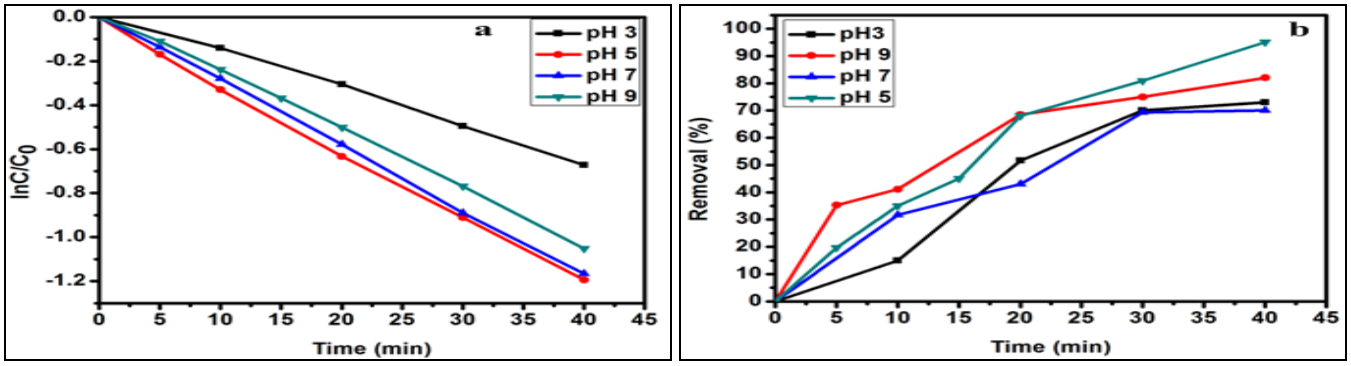

FIG. 9: (a) lN (C_0/C) *vs.* IRRADIATION TIME IN MG, (b) PHOTODEGRADATION EFFICIENCY OF MG

Similar kind of report is shown by Thu *et al.*, [23]. The degradation yields of the cationic dyes are greater in the acidic medium than in neutral and alkaline media, which is correlated with the adsorption behavior of dyes on the catalyst surface. It shows that the degradation of malachite green followed the rate constant, 0.481×10^{-2} min^{-1} (R^2 = 0.9925). **Fig. 9b** illustrates the photodegradation efficiency of ThO_2/Fe_3O_4 nano-composite in which 99.53% of degradation is possible at pH 5.

Effect of Amount of Catalyst: The amount of photocatalyst is another factor affecting the performance of the photocatalyst. The photo-catalytic study was conducted under the following conditions: a source of irradiation, visible light, type of photocatalyst (ThO_2/Fe_3O_4 photocatalyst), the weight of photocatalyst (0.1 g to 0.5 g) and concentration of MG dye solution (2×10^{-5} M). The effect of the loading of the ThO_2/Fe_3O_4 heterogeneous photocatalyst on the degradation of MG dye is shown in **Fig. 10**. The results reveal that the photocatalytic activity increased 80-95% after 40 min by increasing the weight of the ThO_2/Fe_3O_4 photocatalyst from 0.1 to 0.5 g/L due to increased. The degree of decomposition reaction increases with the increase in the reactive sites on the catalyst, beyond which, it shows that the degradation process is reduced, because of the scattering of light. There is a decrease in the penetration of light in the solution. When the amount of catalyst is higher in the solution, the activated molecules get deactivated by the collision of the lower energy molecules thereby increasing the turbidity of the medium and reduction in penetration of light leads to decrease in the rate of the reaction. Also, when the photocatalyst absorbs the highest light; hence, the surface area becomes high, as a result of agglomeration at higher concentration of catalyst.

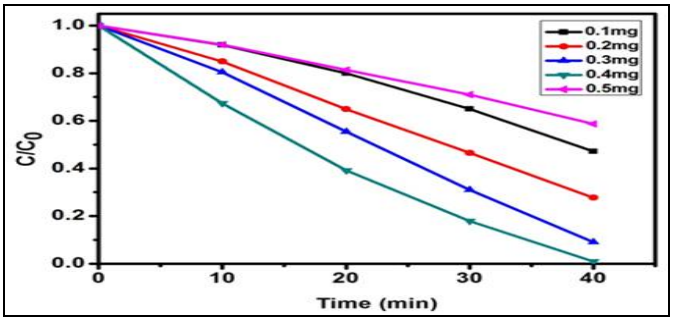

FIG. 10: EFFECT OF CATALYST DOSE ON PHOTO-DEGRADATION OF MG IN AQUEOUS SOLUTION

Plausible Mechanism of MG Dye Degradation: The mechanism of MG dye degradation is initiated by the attack of OH radicals on the malachite green cation. First, the N-demethylation occurs on the attack of OH radicals, leading to the removal of all the four methyl groups present in MG dye.

As there is a continuous generation of OH radicals in the reaction system, the attack of OH radicals occurs spontaneously on the organic moiety. On further reaction, the by-products may undergo continuous degradation due to OH radical attack to bring about a benzene ring removal and ring opening to completely mineralize the material to yield carbon dioxide and water as the end by-products [24, 25, 26]. A schematic representation is shown in **Scheme 1**. **Table 2** shows a comparison of previously reported MG degradation with different photocatalysts [27, 28, 29, 30].

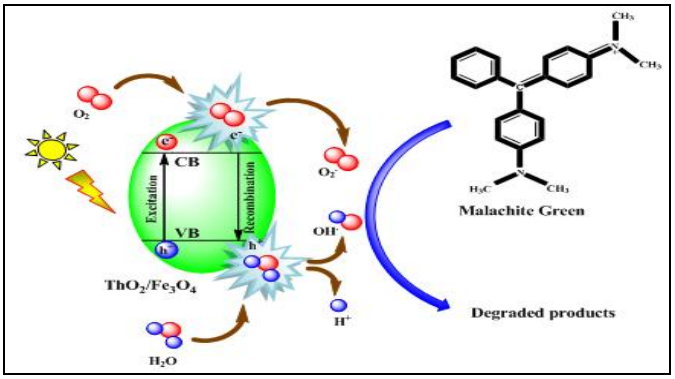

SCHEME 1: MECHANISM FOR THE DEGRADATION OF MG USING ThO_2/Fe_3O_4 NANOCOMPOSITE

TABLE 2: COMPARISON OF PHOTOCATALYTIC DEGRADATION OF MG USING VARIOUS CATALYSTS

MG concentration	Photocatalysts	Weight of catalyst	Time (min)	Degradation %	Reference
20 ml, 100 ppm	α-Fe_2O_3/SnO_2	40 mg	360	86	27
10^{-5} M	PANI/ZnO	0.4 g/L	300	99	28
2×10^{-5} M	$CeFeO_3$	0.05 g	120	91	29
0.05 to 0.4 gL^{-1}	ZnO	0.2 gL^{-1}	-	93.75	30
2×10^{-5} M	ThO_2/Fe_3O_4	0.5g	40	99.53	Present work

Recyclability: The stability of a photocatalyst during the photocatalytic reaction is an important factor for a possible industrial application. To analyze the stability of the photocatalyst, prolonged recycling studies were performed. **Fig. 11** shows the results of the repeated runs of MG degradation using the same photocatalyst. After each cycle, the photocatalyst was collected by centrifugation and then washed with distilled water until the complete removal of dye from the catalyst. Then, the catalyst was dried at 100 ºC overnight and used for another cycle. The photocatalytic activity was found to be nearly the same up to five cycles.

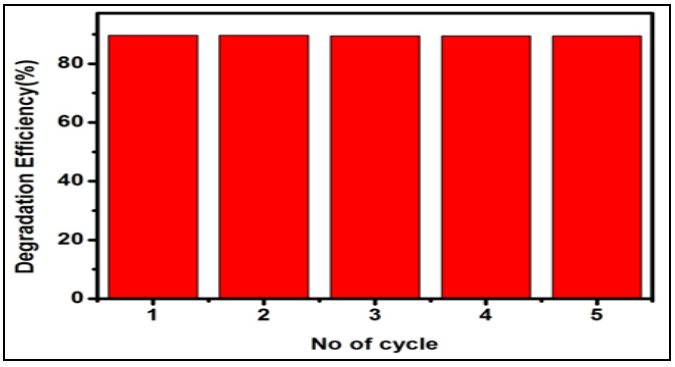

FIG. 11: REUSABILITY STUDY OF ThO_2/Fe_3O_4 CATALYST ON THE PHOTODEGRADATION OF MG

CONCLUSION: In this work, the ThO_2/Fe_3O_4 nanocomposite was prepared and investigated as effective material for removing MG from aqueous solution. Various characterization tools such as XRD, TEM strongly evidence the formation of ThO_2/Fe_3O_4 nanocomposite. Photocatalytic degradation of MG was 99.53% within 40 min. The photocatalyst was reused up to five cycles without significant change in the photocatalytic activity, which indicates the stability of the photo-catalyst. The ThO_2/Fe_3O_4 nanocomposite has a better specific surface area, more reactive sites, and higher stability. The facile preparation method and removal properties for MG imply the promising future of ThO_2/Fe_3O_4 nanocomposite in the practical application for wastewater treatment.

ACKNOWLEDGEMENT: The authors thank the management of Thiagarajar College for providing lab facilities.

CONFLICT OF INTEREST: There is no conflict of interest.

REFERENCES:

1. Ventura-Camargo BC and Marin-Morales MA: Azo dyes: characterization and toxicity- A review. Textiles and Light Industrial Science and Technology 2013; 2: 85-03.
2. Kyzas GZ, Fu J and Matis KA: The change from past to future for adsorbent materials in the treatment of dyeing wastewaters. Materials 2013; 6: 5131-58.
3. Zhong M, Meng X, Wu F, Li J and Fang Y: Mo doping-enhanced dye absorption of Bi_2Se_3 nanoflowers. Nano-scale Research Letters 2013; 8: 451-56.
4. Sharma YC: Adsorption characteristics of a low cost activated carbon for the reclamation of colored effluents containing malachite green. Journal of Chemical & Engineering Data 2011; 56: 478-84.
5. Shi H, Li W, Zhong L and Xu C: Methylene blue adsorption from aqueous solution by magnetic

cellulose/graphene oxide composite: Equilibrium, kinetics, and thermodynamics. Industrial & Engineering Chemistry Research 2014; 53: 1108-18.

6. Saha S, Wang JM and Pal A: Nanosilver impregnation on commercial TiO_2 and a comparative photocatalytic account to degrade malachite green. Separation and Purification Technology 2012; 89: 147-59.
7. Ameta R, Benjamin S, Ameta A and Ameta SC: Photo-catalytic degradation of organic pollutants: a review. Materials Science Forum 2013; 734: 247-72.
8. Serpone N and Emeline AV: Semiconductor photo-catalysis past, present and future outlook. The Journal of Physical Chemistry Letters 2012; 3: 673-77.
9. Wang L, Zhao R, Wang X, Mei L, Yuan L, Wang S, Chaia Z and Shi W: Size-tunable synthesis of monodisperse thorium dioxide nanoparticles and their performance on the adsorption of dye molecules. Cryst Eng Comm 2014; 16: 10469-175.
10. Nkou BGI, Clavier N, Podor R, Cambedouzou J, Mesbah A, Brau HP, Lechelle J and Dacheux N: Preparation and characterization of uranium oxides with spherical shapes and hierarchical structures. Cryst Eng Comm 2014; 16: 6944-54.
11. Wang L, Zhao R, Gu Z, Zhao YL, Chai ZF and Shi WQ: Growth of uranyl hydroxide nanowires and nanotubes by the electrodeposition method and their transformation to One-dimensional U3O8 nanostructures. European Journal of Inorganic Chemistry 2014; 1158-64.
12. Wang L, Zhao R, Wang X, Mei L, Yuan L, Wang X, Chaia Z and Shi W: Size-tunable synthesis of monodisperse thorium dioxide nanoparticles and their performance on the adsorption of dye molecules. Cryst Eng Comm 2014; 16: 10469-475.
13. Liu C, Huang H, Du X, Zhang T, Tian N, Guo Y and Zhang Y: *In-situ* Co-crystallization for the fabrication of g-C_3N_4/Bi_5O_7I heterojunction for enhanced visible-light photocatalysis. Journal of Physical Chemistry C 2015; 119(30): 17156-65.
14. 14. Chen H and Wang L: Nanostructure sensitization of transition metal oxides for visible-light photocatalysis. Beilstein Journal of Nanotechnology 2014; 5: 696-10.
15. Pradhan GK, Hemalata Reddy K and Parida KM: Facile fabrication of mesoporous α-Fe_2O_3/SnO_2 nano hetero-structure for photocatalytic degradation of malachite green. Catalysis Today 2014; 224: 171-79.
16. Polshettiwar V, Luque R, Fihri A, Zhu H, Bouhrara M and Basset J: Magnetically Recoverable Nanocatalysts. Chemcal Reviews 2011; 111: 3036-75.
17. Mahadavi M, Ahmad MB, Haron ML, Gharayebi Y, Shameli K and Nadi B: Fabrication and Characterization of SiO_2/(3-Aminopropyl) triethoxysilane-coated magnetite nanoparticles for lead (II) removal from aqueous solution. Journal of Inorganic and Organometallic Polymers and Materials 2013; 23: 599-07.
18. Pei Y, Han Q, Tang L, Zhao L and Wu L: Fabrication and characterization of hydrophobic magnetite composite nanoparticles for oil/water separation. Materials Technol 2016; 31: 38-43.
19. Karimzadeha I, Dizajia HR and Aghazadeh M: Development of a facile and effective electrochemical strategy for preparation of iron oxides (Fe_3O_4 and γ-Fe_2O_3) nanoparticles from aqueous and ethanol medium and *in-situ* PVC coating of Fe_3O_4 superparamagnetic nanoparticles for biomedical applications. Journal of Magnetism and Magnetic Materials 2016; 416: 81-88.
20. Nigam S, Barick KC and Bahadur D: Development of citrate-stabilized Fe_3O_4 nanoparticles: Conjugation and release of doxorubicin for therapeutic applications. Journal of Magnetism and Magnetic Materials 2011; 323: 237-43.
21. Tan P, Xie X-Y, Liu X-Q, Pan T, Gu C, Chen P-F, Zhou JY, Pan Y and Sun LB: Fabrication of magnetically responsive HKUST-1/Fe_3O_4 composites by dry gel conversion for deep desulfurization and denitrogenation. Journal of Hazardous Materials 2017; 321: 344-52.
22. Ju YM, Yang SG, Ding YC, Sun C, Zhang AQ and Wang LH: Visible light induced photoreduction of methyl orange by N-doped mesoporous titania. Journal of Physical Chemistry A 2008; 112: 11172-77.
23. Thu TNT, Thi NN, Quang VT, Honga KN, Minh TN and Thi Hoai NL: Synthesis, characterization, and effect of pH on degradation of dyes copper-doped TiO_2. Journal of Experimental Nanoscience 2016; 11: 226-38.
24. Wang J, Gao F, Liu Z, Qiao M, Niu X, Zhang K and Huang X: Pathway and molecular mechanism for malachite green biodegradation in *Exiguobacterium sp*. MG2. Plos One 2012; 12: 1-10.
25. Ju Y, Yang S, Ding Y, Sun C, Zhang A and Wang L: Microwave-assisted rapid photocatalytic degradation of malachite green in TiO_2 suspensions: Mechanism and pathways. Journal of Physical Chemistry A 2008; 112: 11172-77.
26. Jain A and Ameta SC: Photocatalytic degradation of malachite green using TiO_2 as photocatalyst. International Journal of Chemical Sciences 2012; 10(4): 1925-33.
27. Pradhan GK, Reddy KH and ParidaKM: Facile fabrication of mesoporous α- Fe_2O_3/SnO_2 nano heterostructure for photocatalytic degradation of malachite green. Catalysis Today 2014; 224: 171-79.
28. Eskizeybek V, Sar F, Gulce H, Gulce A and Ahmet A: Preparation of the new polyaniline/ZnO nanocomposite and its photocatalytic activity for degradation of methylene blue and malachite green dyes under UV and natural sun lights irradiations. Applied Catalysis B: Environmental 2012; 119-120: 197- 06.
29. Ameta KL, Papnai N and Ameta R: Photocatalytic degradation of malachite green using nano-sized cerium-iron oxide. Orbital: Electronic J of Chem 2014; 6: 14-19.
30. Saikia L, Bhuyan D, Saikia M, Malakar B, Dutta DK and Sengupta P: Photocatalytic performance of ZnO nano-materials for self sensitized degradation of Malachite Green dye under solar light. Applied Catalysis A 2015; 490: 42-49.

How to cite this article:
Arumugam R, Periakaruppan P and Selvanathan R: A facile novel synthesis of ThO_2/Fe_3O_4 nanocomposite with enhanced photocatalytic activity for the degradation of malachite green under visible light irradiation. Int J Pharm Sci & Res 2019; 10(6): 2902-10. doi: 10.13040/IJPSR.0975-8232.10(6).2902-10.